SUPPORTING INFORMATION for

# Effect of springtime thermal forcing over Tibetan Plateau on summertime ozone in Central China during the period 1950–2019

Yuexuanzi Wang [1#], Yingying Yan [1#*], Kunyu Duan [1], Shaofei Kong [1, 2], Jintai Lin[3], Huang Zheng [1, 4], Aili Song [1], Zexuan Zhang [1, 4]

[1] Department of Atmospheric Science, School of Environmental Sciences, China University of Geosciences, Wuhan, 430074, China

[2] Research Centre for Complex Air Pollution of Hubei Province, Wuhan 430078, China

[3] Laboratory for Climate and Ocean-Atmosphere Studies, Department of Atmospheric and Oceanic Sciences, School of Physics, Peking University, Beijing 100871, China

[4] Department of Environmental Science and Engineering, School of Environmental Studies, China University of Geosciences, Wuhan, 430074, China

## S1. Comparison of NCEP/NCAR and ERA5 data

In order to verify the reliability of the NCEP/NCAR Reanalysis data, we have used the ERA5 data to conduct a comparison. The meteorological variables we discussed are from 1950 to 2019, including surface air temperature (1000 hPa), specific humidity (1000 hPa) and horizontal wind fields (1000 hPa, 850 hPa and 500 hPa). The summertime (1950–2019) spatial distributions of the ERA5 meteorological variables (Fig. S11) are similar with those of NCEP/NCAR data (Fig. 3 and Fig. 5). In addition, the differences of each variable averaged over the study period and the high/low TPE years shown in NCEP/NCAR and ERA5 are similar.

## S2. The statistical model of Kolmogorov-Zurbenko (KZ) filter

We use the Kolmogorov-Zurbenko (KZ) filter model to separate the influences of meteorology and emission-related trends.

$$X_{LT}(t) = X_{LT}^{EMI}(t) + X_{LT}^{MET}(t)$$

Where $X_{LT}$ means the long-term component, $X_{LT}^{EMI}$ means emission-related long-term components, and $X_{LT}^{MET}$ means meteorology-related long-term series. The slope of the linear regression between time series and components represent the linear trends (Seo et al., 2018). The factors we considered include surface air temperature, surface relative humidity, sea level pressure, horizontal wind fields and daily precipitation.

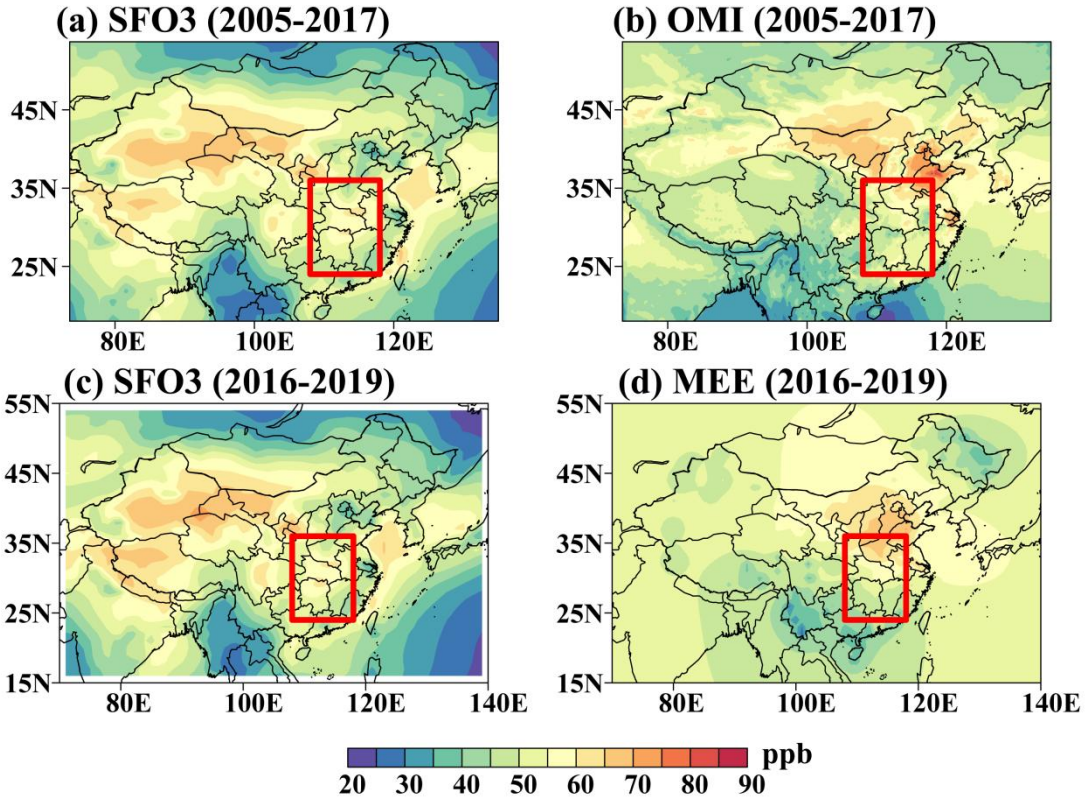



**Figure S1.** Spatial distribution of summertime surface ozone averaged over 2005–2017 based on CMIP6 data (a) and OMI observation (b). Spatial distribution of summertime surface ozone averaged over 2016–2019 based on CMIP6 data (c) and station observations (noontime ozone between 12:00 and 15:00 based on 8-hour moving averages) (d). The red frame draws the area of Central China (108–118°E, 24–36°N).

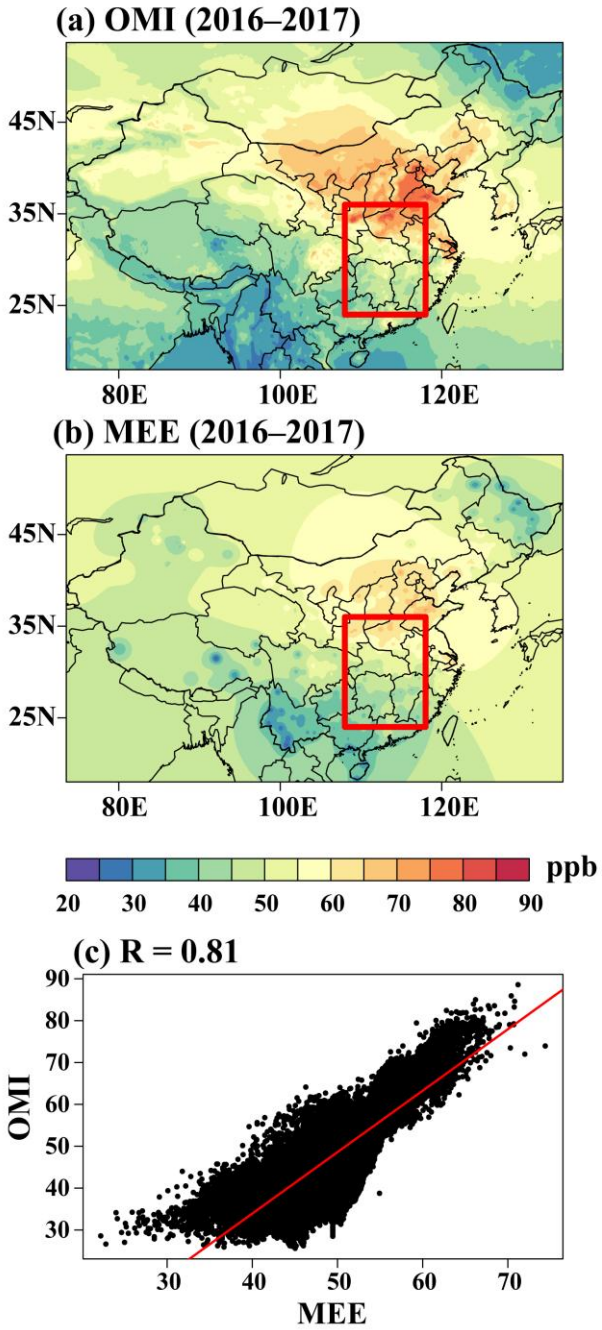



**Figure S2.** Spatial distribution of summertime surface ozone averaged over 2016–2017 based on OMI (a) and MEE observation (b). The red frame draws the area of Central China. (c) The correlation between OMI and MEE over entire China from 2016 to 2017 ($R = 0.81$, P-value $< 0.05$).

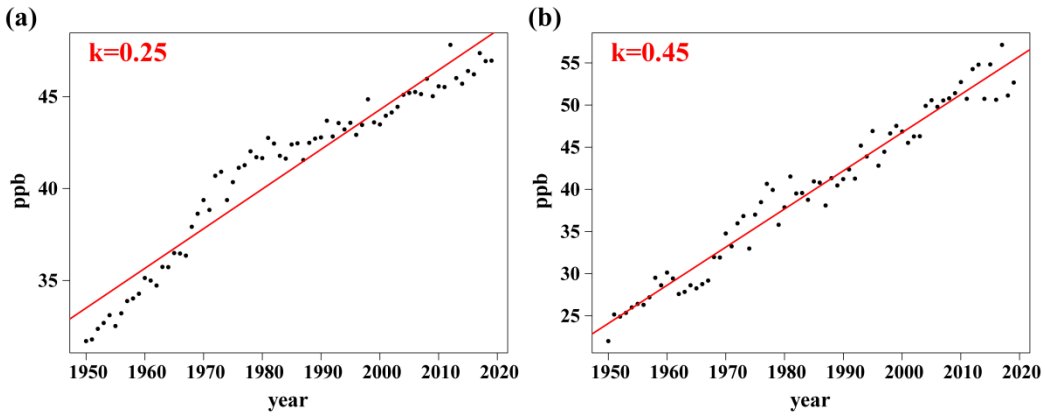



**Figure S3.** (a) The emission-related trend is 0.25 ppb $yr^{-1}$ over entire China during 1950–2019 calculated by the CMIP6 data. (b) The emission-related trend is 0.45 ppb $yr^{-1}$ during 1950–2019 over Central China calculated by the CMIP6 data.

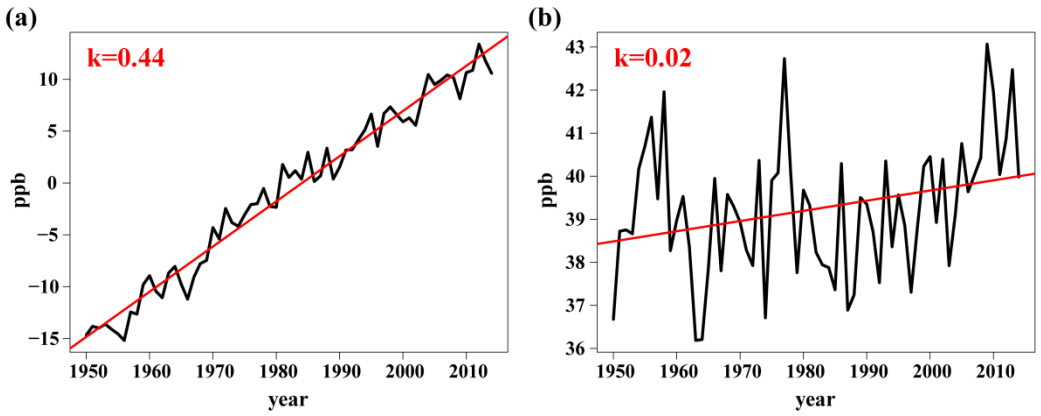



**Figure S4.** (a) The effects of anthropogenic emission changes on surface ozone trend according to Kolmogorov-Zurbenko (KZ) filter model (0.44 ppb $yr^{-1}$). (b) The effects of climate variability on surface ozone trend according to Kolmogorov-Zurbenko (KZ) filter model (0.02 ppb $yr^{-1}$).

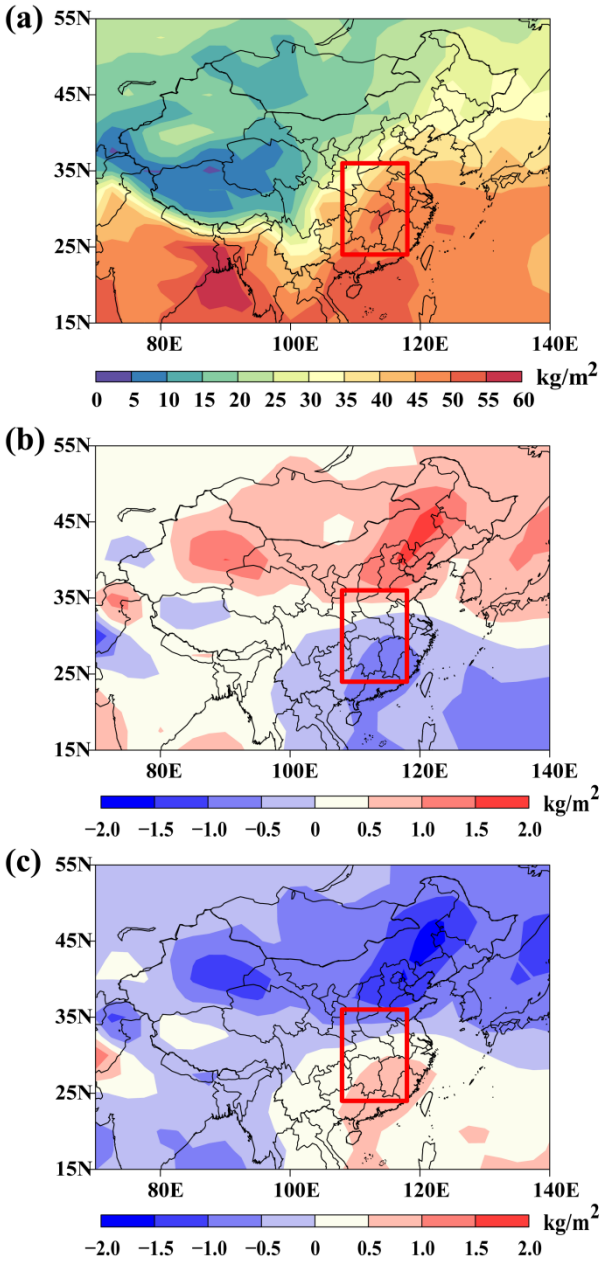



**Figure S5.** The spatial distribution of surface precipitation (a). The difference of summertime surface precipitation over the study period (1950–2019) and the high/low (b/c) TPE years. The red frame draws the area of Central China.

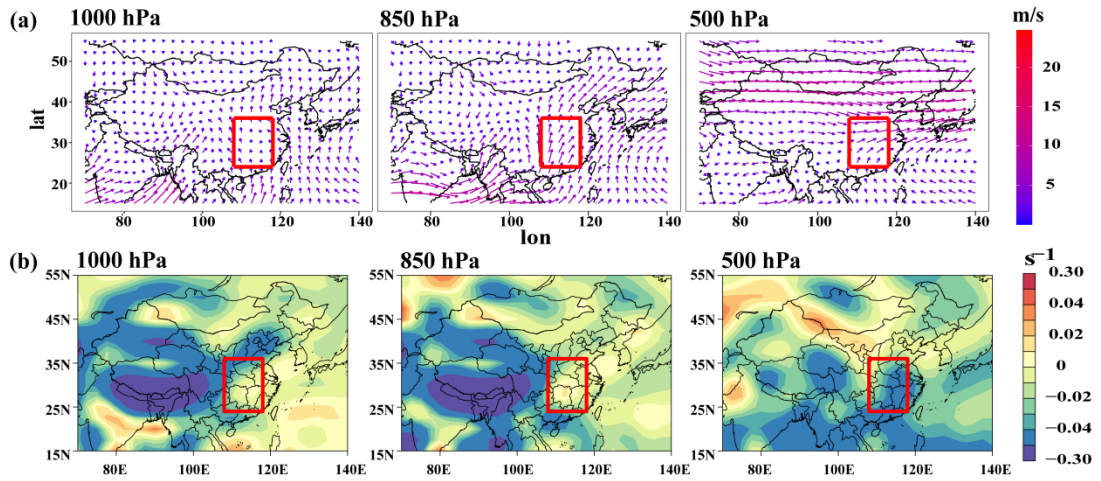



**Figure S6.** (a) The summertime horizontal wind fields at 1000 hPa, 850 hPa and 500 hPa in high TPE years. (b) The summertime vertical velocity at 1000 hPa, 850 hPa and 500 hPa in high TPE years. The red frame draws the area of Central China.

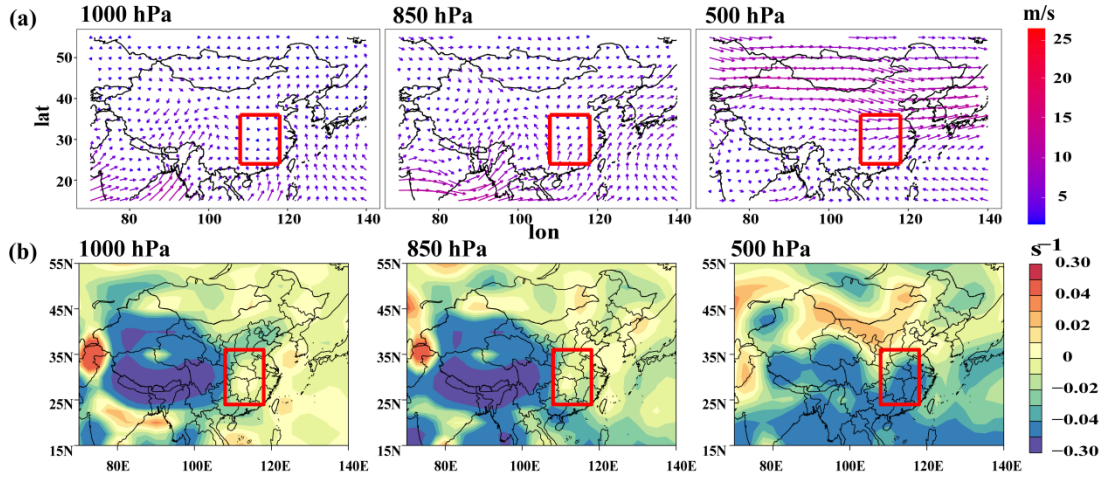



**Figure S7.** (a) The summertime horizontal wind fields at 1000 hPa, 850 hPa and 500 hPa in low TPE years. (b) The summertime vertical velocity at 1000 hPa, 850 hPa and 500 hPa in low TPE years. The red frame draws the area of Central China.

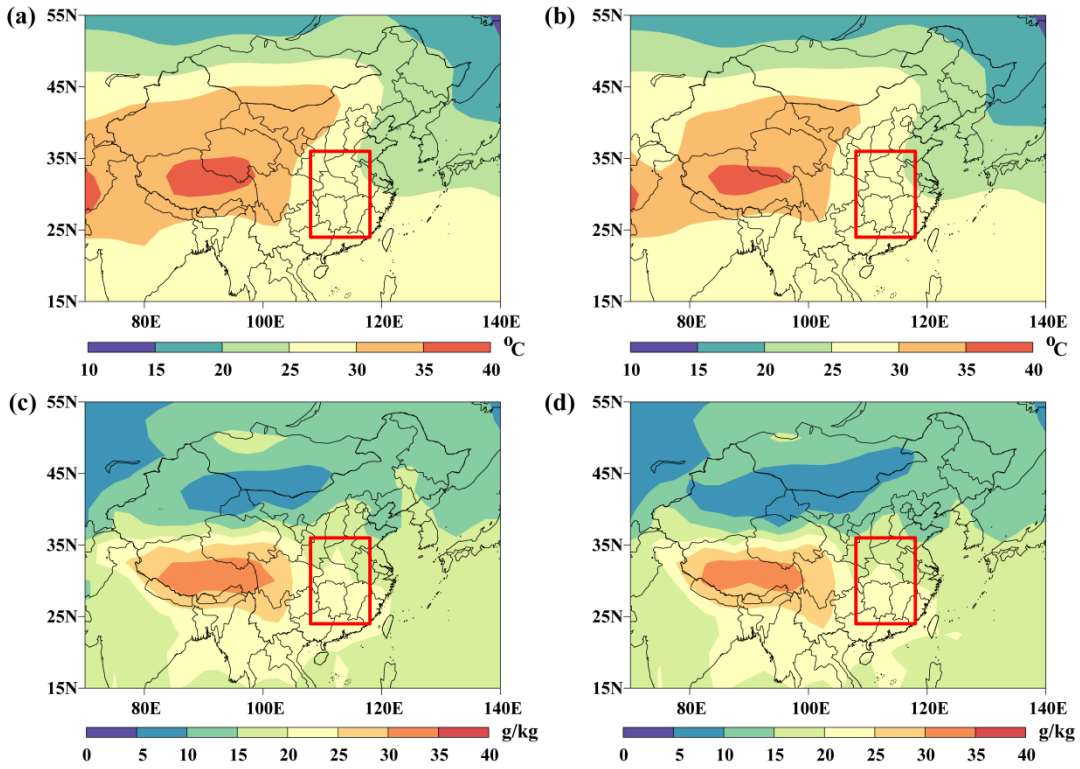



**Figure S8.** The summertime surface air temperature (1000 hPa) in high TPE years (a) and low TPE years (b). The summertime specific humidity (1000 hPa) in high TPE years (c) and low TPE years (d). The red frame draws the area of Central China.

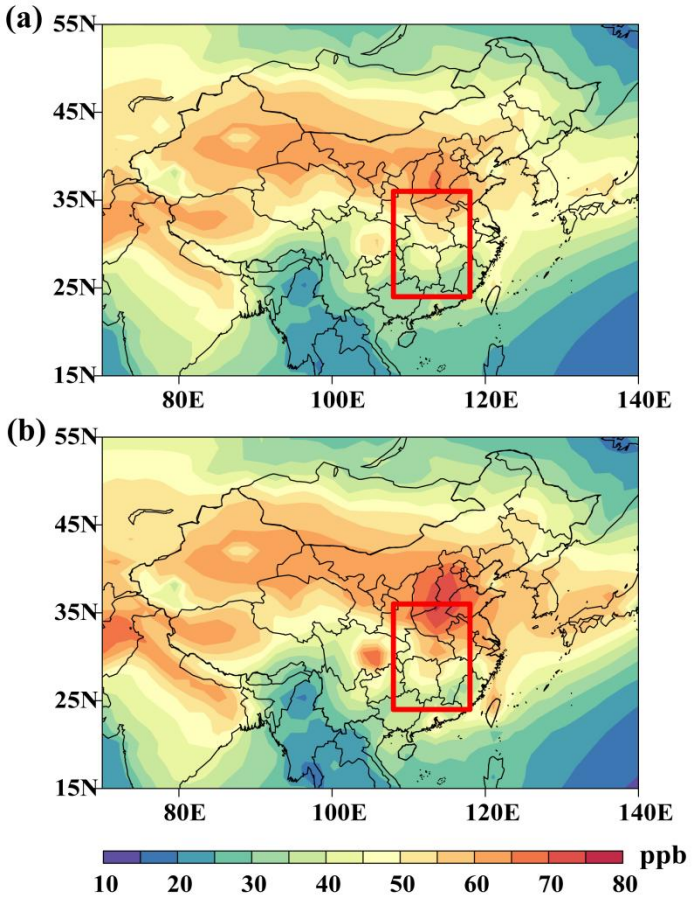



**Figure S9.** The summertime surface ozone concentrations in high TPE years (a), low TPE years (b). The red frame draws the area of Central China.

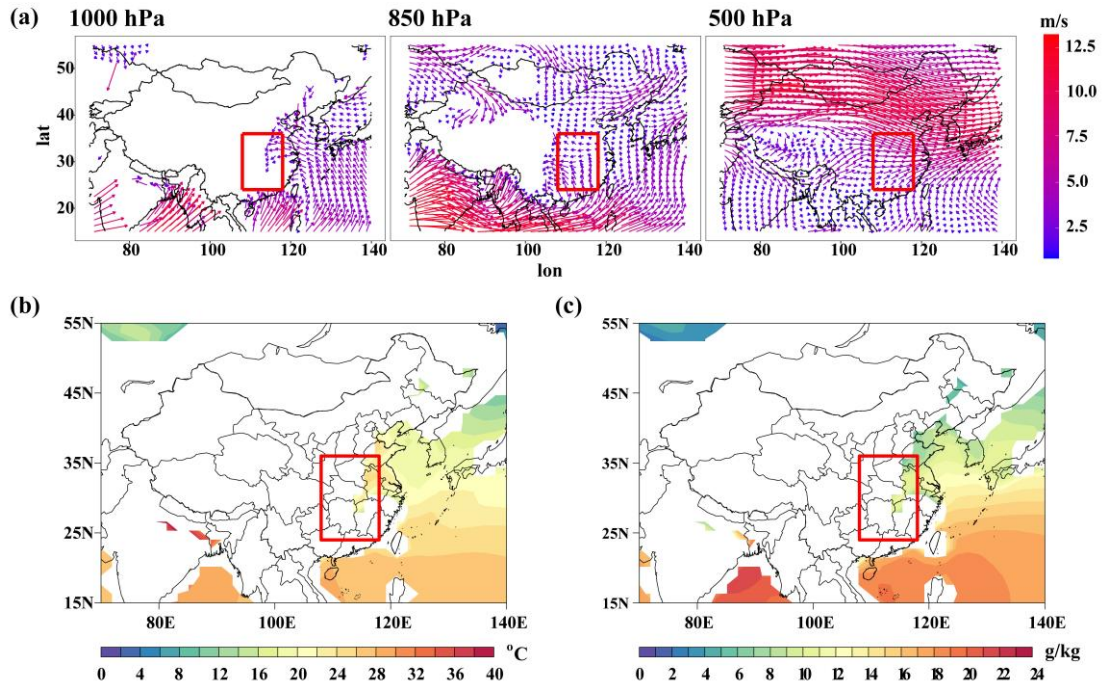



**Figure S10.** For CMIP6, the spatial distribution of horizontal wind fields at 1000 hPa, 850 hPa and 500 hPa (a), surface air temperature at 1000 hPa (b) and specific humidity at 1000 hPa (c). The red frame draws the area of Central China.

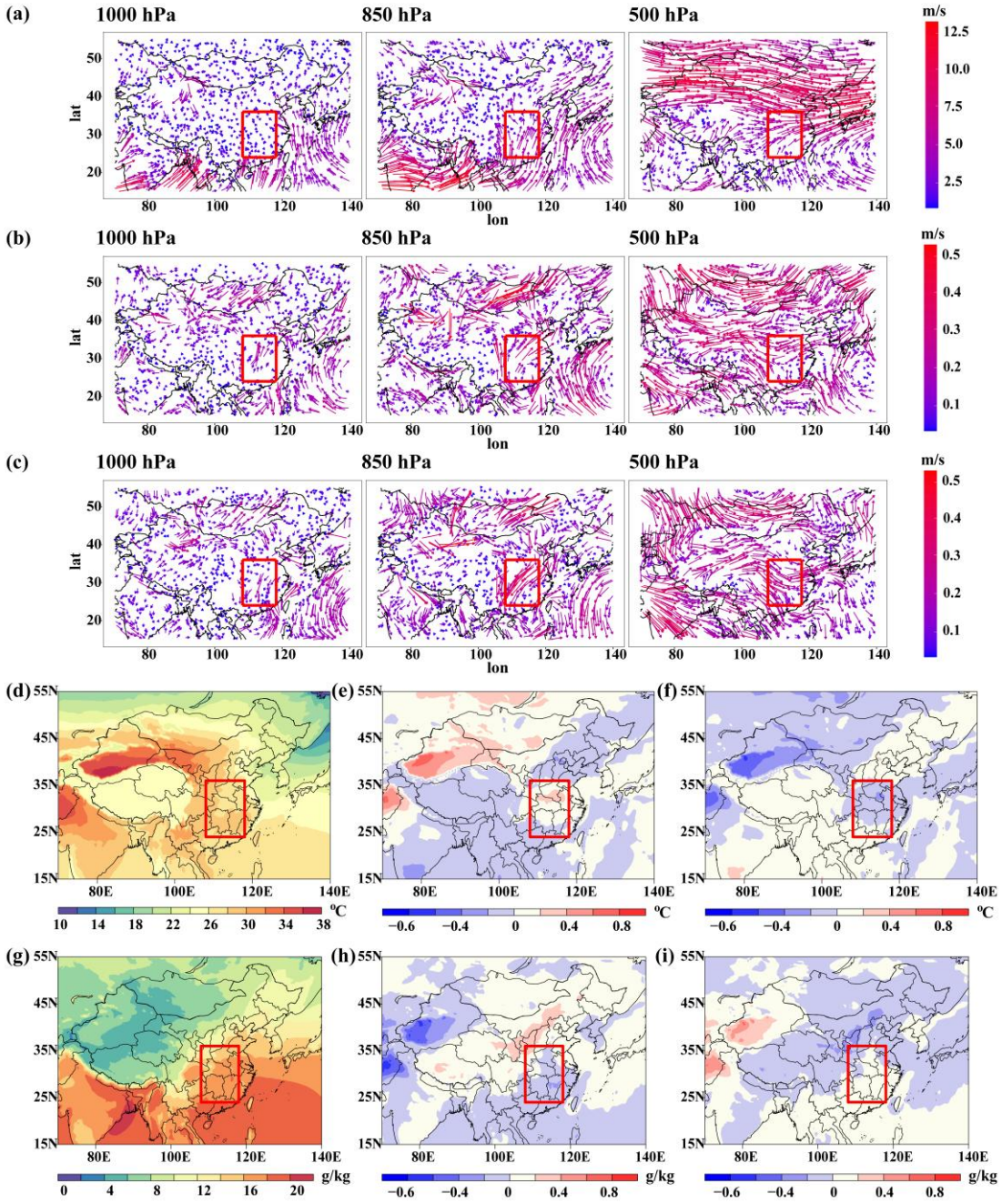



**Figure S11.** For ERA5, the spatial distribution of horizontal wind fields at 1000 hPa, 850 hPa and 500 hPa (a), surface air temperature at 1000 hPa (d) and specific humidity at 1000 hPa (g). The difference of summertime horizontal wind fields, surface air temperature and specific humidity averaged over the study period (1950–2019) and the high/low (b/c; e/f; h/i) TPE years. The red frame draws the area of Central China.

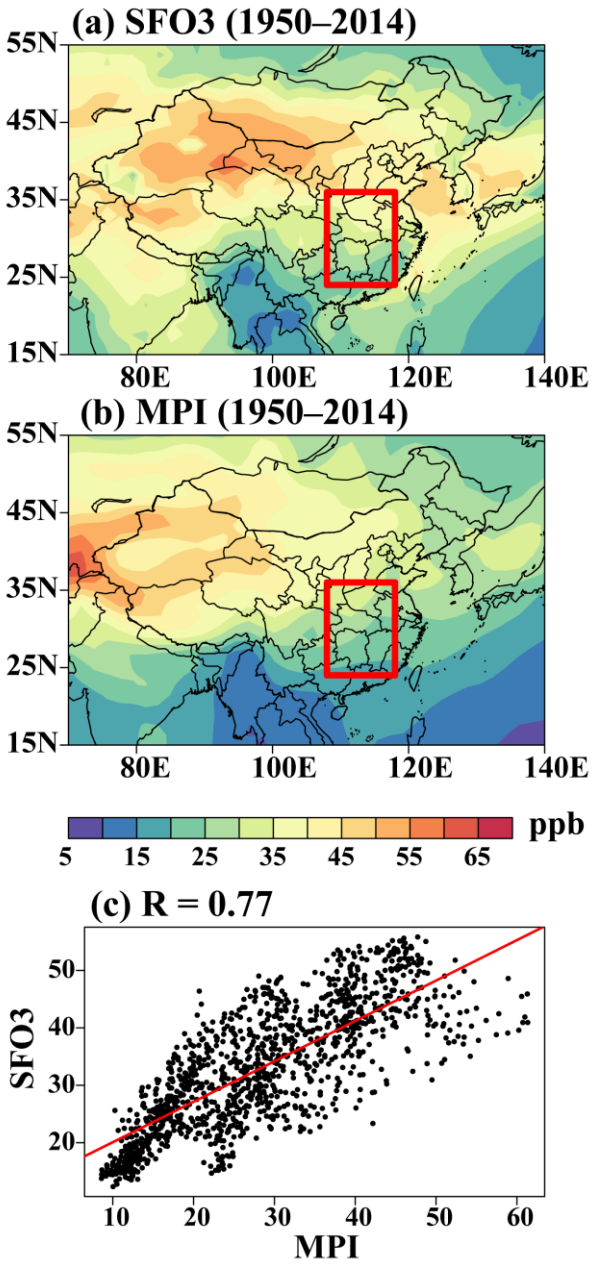



**Figure S12.** Spatial distribution of summertime surface ozone averaged over 1950–2014 based on SFO3 (modeled surface ozone data from the CMIP6 UKESM1-0-LL) (a) and MPI (modeled surface ozone data from the CMIP6 MPI-ESM-1-2-HAM) (b). The red frame draws the area of Central China. (c) The correlation between SFO3 and MPI over entire China from 1950 to 2014 ($R = 0.77$, P-value $< 0.05$).